Contents lists available at ScienceDirect

Process Safety and Environmental Protection

journal homepage: www.elsevier.com/locate/psep

Visible light TiO_2 photocatalysts assessment for air decontamination

M.M. Ballari[a,*], J. Carballada[a], R.I. Minen[a], F. Salvadores[a], H.J.H. Brouwers[b], O.M. Alfano[a], A.E. Cassano[a,1]

[a] INTEC (Universidad Nacional del Litoral and CONICET), Ruta Nacional N° 168. Km. 472, 5, 3000 Santa Fe, Argentina

[b] Department of the Built Environment, Eindhoven University of Technology, P.O. Box 513, 5600 MB Eindhoven, The Netherlands

ARTICLE INFO

Article history:
Received 20 March 2015
Received in revised form 19 July 2015
Accepted 4 August 2015
Available online 19 August 2015

Keywords:
Visible light
Photocatalysis
Air purification
Nitrogen oxide
Acetaldehyde
Efficiency

ABSTRACT

Different visible light responses of commercial TiO_2 photocatalysts are assessed for their application in air decontamination. To do that the modified TiO_2 catalysts were immobilized on borosilicate glass plates according to a dip coating method. Then, the photocatalytic performance of these plates was evaluated in a continuous gas flat plate photoreactor irradiated with visible light lamps using two representative air pollutants: nitrogen oxide and acetaldehyde. Working under visible light, the modified TiO_2 catalysts were compared by means of efficiency parameters: the true quantum efficiency, which relates the moles of degraded pollutant with the moles of the absorbed photons, and the apparent photonic efficiency, which relates the moles of degraded pollutant with the moles of incident photons. Also, the photocatalytic pollutants degradation by immobilized modified TiO_2 could be related with their optical properties, finding a clear correlation between them. These results are useful to decide which TiO_2 will be more efficient for a full scale air decontamination process under visible light illumination.

1. Introduction

Heterogeneous photocatalysis represents an emerging environmental control option for the efficient removal of chemical pollutants that can be applied for water and air purification (Hoffmann et al., 1995). One of the limitations of this technology is that normal TiO_2 can only be activated by UV radiation (280–400 nm) that represents 4% of the total energy of the sun; meanwhile the visible light constitutes 45% of the solar radiation. On the other hand, the UV radiation amounts to only 0.001–0.05 W/m^2 in indoor lighting (Kuo et al., 2007). To extend the use of photocatalysis to visible light region, it is necessary to prolong TiO_2 radiation absorption to wavelengths corresponding to visible spectrum (400–700 nm). So far, several modification methods of photocatalyst to amplify its absorption spectrum to visible radiation have been investigated and therefore, the applicability of heterogeneous photocatalysis has been extended (Banerjee et al., 2014; Chatterjee and Dasgupta, 2005; Daghrir et al., 2013; Kisch and Macyk, 2002). Several commercial types of modified TiO_2 can be already found in the market for indoor visible light applications.

There are various types of modified TiO_2 active under visible light and different methods to perform the modification process. A first method is the treatment of TiO_2 with reductive hydrogen plasma (Van Durme et al., 2007). TiO_2 can also be sensitized by adsorbed dyes and semiconductors having lower band-gaps and more cathodic conduction bands (Demeestere et al., 2005). A third method is the TiO_2 doping with

* *Corresponding author*. Tel.: +54 342 4511546; fax: +54 342 4511087.
E-mail address: ballari@santafe-conicet.gov.ar (M.M. Ballari).
[1] Deceased July 12, 2014.
http://dx.doi.org/10.1016/j.psep.2015.08.003
0957-5820/

transition metals such as Fe, Cu, Co, Ni, Cr, V, Mn, Mo, Nb, W, Ru, Pt and Au (He et al., 2010). Finally, an alternative approach is the doping with non-metal anions, like nitrogen (Jo and Shin, 2010), carbon (Kuo et al., 2007) or sulphur (Nishijima et al., 2007).

In many studies employing modified TiO_2 with visible light absorption, the photocatalytic degradation of several volatile organic compounds (VOCs) and inorganic gases has been studied: nitrogen oxides (Yu and Brouwers, 2009; Lin et al., 2006; Nakamura et al., 2000), 2-propanol (Ihara et al., 2001), toluene (Fuerte et al., 2001; Ihara et al., 2001; Kubacka et al., 2009; Van Durme et al., 2007), acetaldehyde (Asahi et al., 2001; Iketani et al., 2004; Nishijima et al., 2007; Sakthivel and Kisch, 2003a, 2003b), acetone (Ihara et al., 2003), benzene (Sakthivel and Kisch, 2003a,b), carbon monoxide (Sakthivel and Kisch, 2003a,b), trichloroethylene (Demeestere et al., 2005; Jo and Yang, 2010), dimethyl sulfide (Demeestere et al., 2005) and dimethyl disulphide (Jo and Shin, 2010), methyl-tertiary butyl ether (Jo and Yang, 2010), acetic acid (Nishijima et al., 2007), and formic acid (Nishijima et al., 2007).

In the present work, different visible light absorption TiO_2 commercially available catalysts, one doped with carbon, another doped with nitrogen and two photocatalytic solutions ready to use, are studied. The carbon doping introduces new states close to the valence band edge of TiO_2 narrowing the photocatalyst band gap. In addition, carbonaceous species at the surface of the photocatalyst facilitates the absorption in the visible wavelengths as well as the high surface area of the doped TiO_2 promotes the adsorption of pollutants. Nitrogen doped titania could have either substitutional or interstitial N atoms in the TiO_2 matrix, resulting in a visible light response due to the electron transition from the localized N orbital to the conduction band or to the surface adsorbed O_2. One of the employed solutions is made of silver modified TiO_2. The noble metal doping increases the separation of photogenerated charge carries and reduces the recombination rate of photoinduced electron–hole pair.

Two representative air pollutants are employed to assess the photocatalytic performance under visible light of the modified TiO_2 mentioned above: (i) NO as an inorganic contaminant and (ii) acetaldehyde as a simple structured organic pollutant. The nitrogen oxides (NO_x) are the generic term for a group of highly reactive gases, most of them emitted to air in the form of nitric oxide (NO) and nitrogen dioxide (NO_2). They are mainly formed in combustion processes and cause a wide variety of health and environmental impacts. The NO_x compounds are responsible for tropospheric ozone and urban smog through photochemical reactions with hydrocarbons. Furthermore, NO_x together with SO_x (sulfur dioxide and sulfur trioxide) is the major contributor to the "acid rain". On the other hand, acetaldehyde is one of toxic, irritant, and probable carcinogen VOC contaminant in indoor and outdoor environments. It is also a result of: (i) combustion processes, such as vehicle exhaust, tobacco smoke, and wood burning, and (ii) sources in homes including building materials, like laminate, linoleum, wooden varnished, and cork/pine flooring, plastic water based and matt emulsions paints, wooden, particleboard, plywood and chipboard furniture (Missia et al., 2010).

The photocatalysts were immobilized on borosilicate glass plates according to a dip coating method. The optical properties of the immobilized samples were determined in order to correlate the visible light absorption with the de-polluting capability. The performance of these systems was evaluated calculating the photonic and the quantum efficiencies, that correlate the contaminant reaction rate with the incident radiation flux and the absorbed radiation by the catalysts, respectively. The main objective of this work is to determine which photocatalyst will present the best pollution abating ability in a full scale application under visible light conditions.

2. Experimental

2.1. *Sample preparation*

Four types of visible light photocatalysts were acquired from the marked: a powder doped with carbon, a powder doped with nitrogen and two liquid solutions ready to use for coatings. The measured BET area for the Carbon and Nitrogen doped TiO_2 powders were 251 $m^2\,g^{-1}$ and 34 $m^2\,g^{-1}$ respectively.

The immobilization of the TiO_2 powders and liquid suspensions was carried out according to a dip coating procedure on borosilicate glass plates. The TiO_2 powders load in deionized water to prepare the coating was 75 $g\,L^{-1}$. For every dip coating cycle, the glass piece was dried at 110 °C for 24 h and calcined at 500 °C for 2 h, repeating this procedure four times. Additionally, in order to increase the adhesion between the TiO_2 particles and glass, especially for employing the carbon doped catalyst, some plates were sandblasted. On the other hand, as the TiO_2 suspensions at natural pH precipitate quite fast, different suspensions at different pHs adjusted with nitric acid and sodium hydroxide were prepared, finding that the suspension at pH 1 for both TiO_2 powders were the most stable. Table 1 summarizes all prepared sample and the corresponding deposited photocatalyst mass per unit area. The given samples names are TiO_2-*m*-*n*L or TiO_2-*m*-*n*L-S, where *m* refers

Table 1 – Prepared samples and main characteristics.

Sample name	Type of catalyst	Number of layers	Glass surface	Suspension pH	Specific load ($g\,cm^{-2}$) × 10^4
TiO_2-C-1 L	Carbon doped TiO_2 powder	1	Smooth	6	3.75
TiO_2-C-4 L		4	Smooth	6	8.02
TiO_2-C-1 L-S		1	Sandblasted	1	1.06
TiO_2-C-4 L-S		4	Sandblasted	1	2.34
TiO_2-N-1 L	Nitrogen doped TiO_2 powder	1	Smooth	6	2.12
TiO_2-N-4 L		4	Smooth	6	4.43
TiO_2-N-1 L-S		1	Sandblasted	1	0.965
TiO_2-N-4 L-S		4	Sandblasted	1	1.53
TiO_2-Ag-Sol-4 L	Silver modified TiO_2 solution	4	Smooth	–	0.280
TiO_2-Sol-4 L	Visible light response modified TiO_2 solution	4	Smooth	–	0.501

to the agent that modifies the TiO_2, *n* is the number of layers (L) of the immobilized sample, and S means sandblasted glass.

In order to assess the stability of the prepared samples, the coatings made with TiO_2-C and TiO_2-N were flushed with water, observing only a mass decreased of the films on the smooth glasses.

2.2. *Optical properties*

The optical properties of the immobilized TiO_2 on the glass plate were determined as a function of wavelength between 300 and 600 nm in an Optronic OL Series 750 spectroradiometer equipped with an OL 740-70 integrating sphere reflectance attachment coated with polytetrafluorethylene (PTFE). To evaluate the fraction of energy absorbed (A) by the TiO_2 film, the spectral diffuse reflectance and the spectral diffuse transmittance of the coated glass were experimentally determined according to the schematic representation made in Fig. 1 (Zacarías et al., 2012).

2.3. *Photocatalytic performance*

The photocatalytic performance of the prepared samples was studied with the degradation of two air contaminants, one inorganic and another one organic, in to some extent quite similar experimental setups. Some operating conditions stated in the ISO standards 22197-1 and 22197-2 (ISO, 2007, 2011) for nitrogen oxide and acetaldehyde degradation

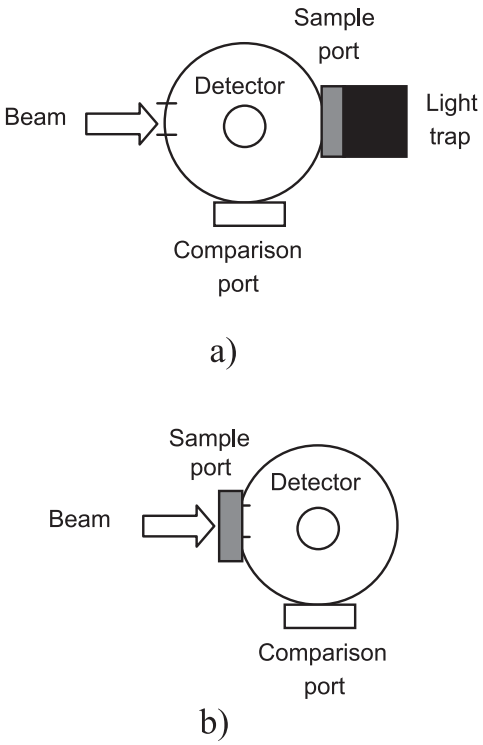

Fig. 1 – Integrating sphere configuration (a) Diffuse reflectance measurement. (b) Diffuse transmittance measurement.

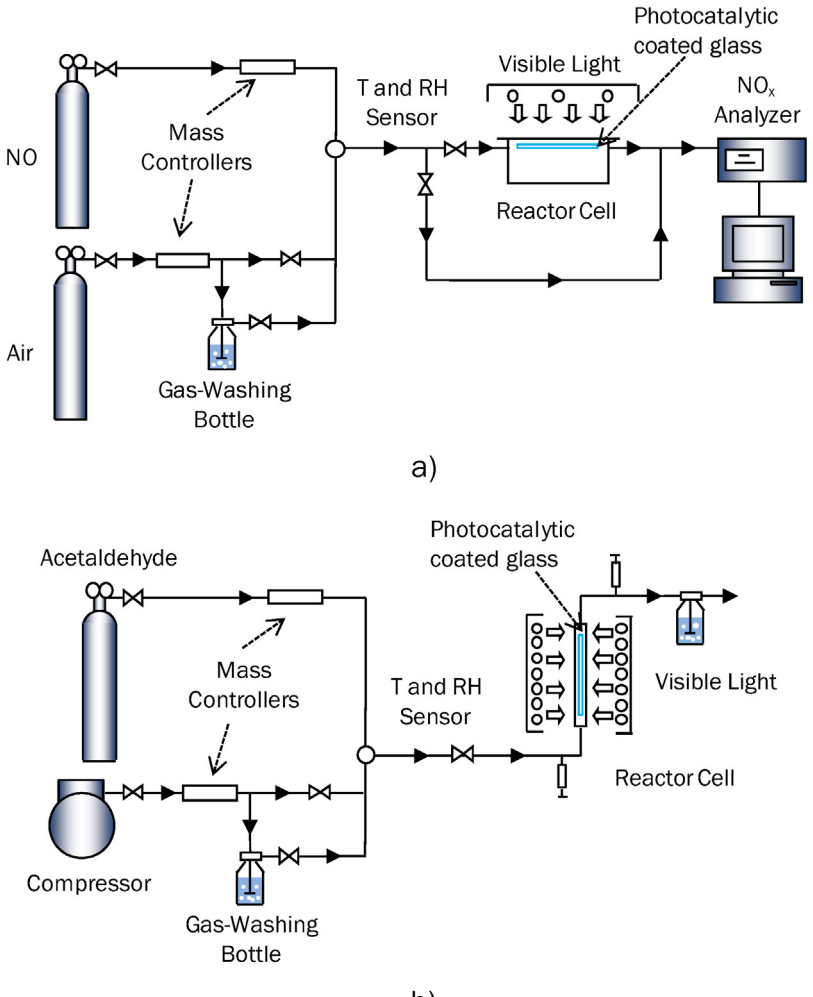

Fig. 2 – Experimental setup. (a) NO degradation, and (b) acetaldehyde degradation.

Table 2 – Experimental setup characteristics and operating conditions.

Contaminant		Nitrogen oxide	Acetaldehyde
Reactor	Length	20 cm	20 cm
	Width	10 cm	10 cm
	Height	0.3 cm	0.2 cm each side
	Volume	60 cm^3	40 cm^3 each side
Photocat. sample	Length	20 cm	20 cm
	Width	10 cm	10 cm
Visible lamps		Philips master TLD 865 × 3	GE F4T5/CW × 14
	Input power	18 W	4 W
	Emission Wavelength	380–720 nm	380–720 nm
Flow rate		3 L min^{-1}	1 L min^{-1}
Temperature		20–23 °C	21–24 °C
Relative humidity		50%	50%
Irradiance flux		10 W m^{-2}	64 W m^{-2} each side
Inlet pollutant concentration		1 ppm	5 ppm

respectively were followed. For the degradation of the inorganic compound (nitrogen oxide), the applied experimental device is composed of a planar reactor cell housing the photocatalytic plate sample, a suitable visible light source, an online chemiluminescent NO_x analyzer and an appropriate gas supply (Fig. 2(a)) (Ballari et al., 2010). The chemiluminescence method uses the reaction of NO with O_3 generating excited NO_2^* molecules that return to the ground state emitting chemiluminescence in the range of 600–3000 nm. The light intensity is proportional to the concentration of NO molecules. On the other hand, a deoxidation converter changes the NO_2 to NO, which is then measured. In other words, the NO_2 concentration can be obtained by the difference between: (i) the NO_x ($NO + NO_2$) concentration measured when the sample gas is directed through a converter and (ii) the NO concentration measured when the gas is not run through the converter.

For the degradation of the organic pollutant (acetaldehyde) a continuous planar photoreactor with similar dimensions to the previous one was also employed, with the difference that here the glass pieces with the immobilized TiO_2 were irradiated on both sides of the photoreactor to improve the photocatalytic degradation of the pollutant. The photocatalytic reactor was fed by acetaldehyde gas stabilized in nitrogen and irradiated with fluorescence visible light lamps (Fig. 2(b)). The outlet and inlet contaminant concentration from the reactor was analyzed employing a gas chromatograph with a FID detector performing a direct injection of the gas sample.

Table 2 shows the main characteristics, dimensions and operating conditions of the experimental setup that were employed to carry out the NO and acetaldehyde photocatalytic degradation experiments.

3. Results and discussion

3.1. *Optical properties*

The results of the diffuse transmittance and reflectance measurements of the prepared samples on the smooth glasses (T_{TiO_2,g,TiO_2} and R_{TiO_2,g,TiO_2} respectively) can be found in Fig. 3. Fig. 4 shows the optical measurements for the sandblasted samples for 1 and 4 layers.

The radiation absorption fraction (A) of the immobilized photocatalyst can be calculated from the measured values of diffuse reflectance (R) and diffuse transmittance (T) of the borosilicate glass alone and coated with TiO_2 on both sides.

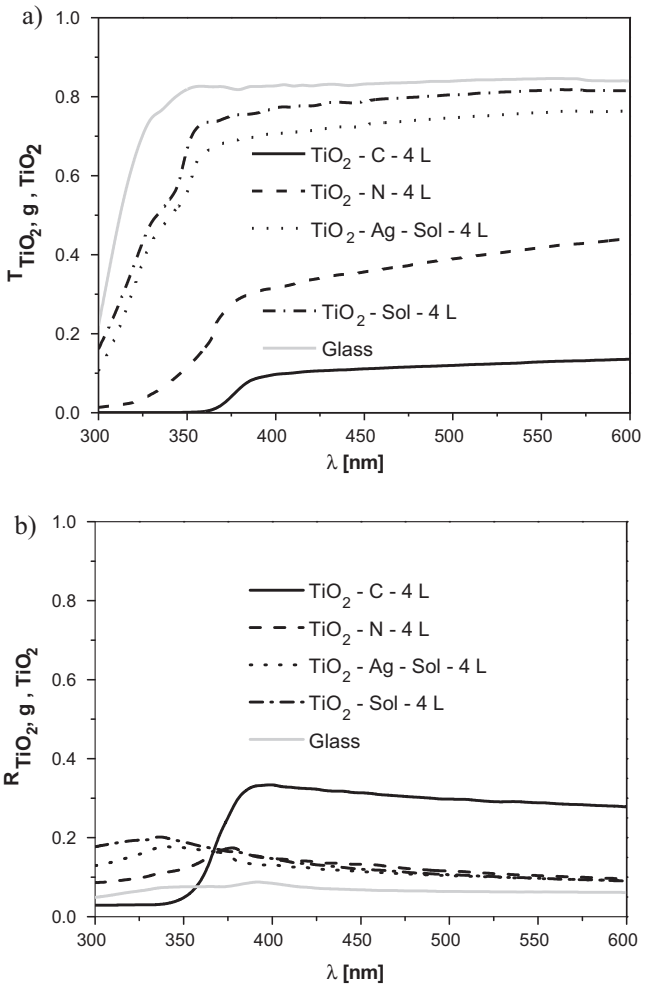

Fig. 3 – Experimental optical properties of smooth coated glass. (a) Diffuse transmittance, and (b) diffuse reflectance.

To do that, a radiative flux balance is applied in each layer of Fig. 5 according to (Edwards, 1977; Siegel and Howell, 2002):

$$q_{n-1}^{-} = T_n q_n^{-} + R_n q_{n-1}^{+} \quad n = 1, 2, 3 \tag{1}$$

or:

$$q_n^{+} = R_n q_n^{-} + T_n q_{n-1}^{+} \quad n = 1, 2, 3 \tag{2}$$

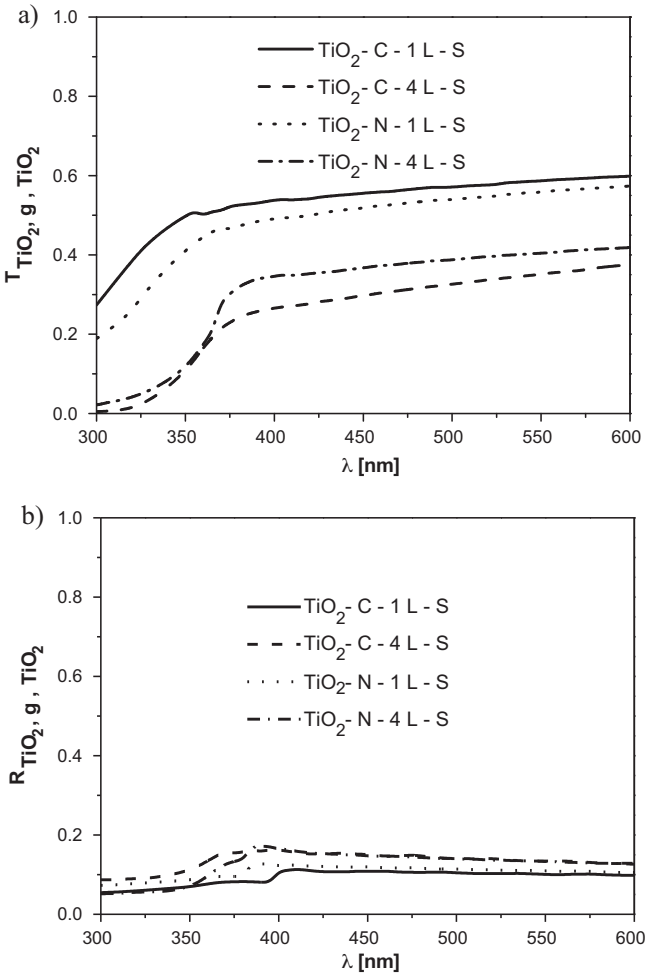

Fig. 4 – Experimental optical properties of sandblasted coated glass. (a) Diffuse transmittance, and (b) diffuse reflectance.

where T_n and R_n are the diffuse transmittance and reflectance of the n^{th} layer respectively; q_n^- and q_n^+ are the net radiation flux going into and out from the n^{th} layer respectively.

Also, considering that:

$$T_{TiO_2,g,TiO_2} = \frac{q_0^-}{q_3^-} \tag{3}$$

$$R_{TiO_2,g,TiO_2} = \frac{q_3^+}{q_3^-} \tag{4}$$

and $R_1 = R_3 = R_{TiO_2}$, $R_2 = R_g$, $T_1 = T_3 = T_{TiO_2}$, and $T_2 = T_g$, the following expressions for the optical properties of the TiO_2 film can be derived (see Appendix A):

$$R_{TiO_2} = \frac{R_{TiO_2,g,TiO_2}T_g - T_{TiO_2,g,TiO_2}R_g}{T_{TiO_2,g,TiO_2}T_g^2 - T_{TiO_2,g,TiO_2}R_g^2 + T_g} \tag{5}$$

$$T_{TiO_2} = \sqrt{\frac{(R_{TiO_2,g,TiO_2} - R_{TiO_2})[1 - R_{TiO_2}(R_g + (T_g^2 R_{TiO_2}/(1 - R_g R_{TiO_2})))]}{R_g + (T_g^2 R_{TiO_2}/(1 - R_g R_{TiO_2}))}} \tag{6}$$

where R_g, R_{TiO_2,g,TiO_2}, T_g, and R_{TiO_2,g,TiO_2} are the experimental diffuse reflectance and transmittance of the borosilicate glass and the coated glass on both side with TiO_2, respectively.

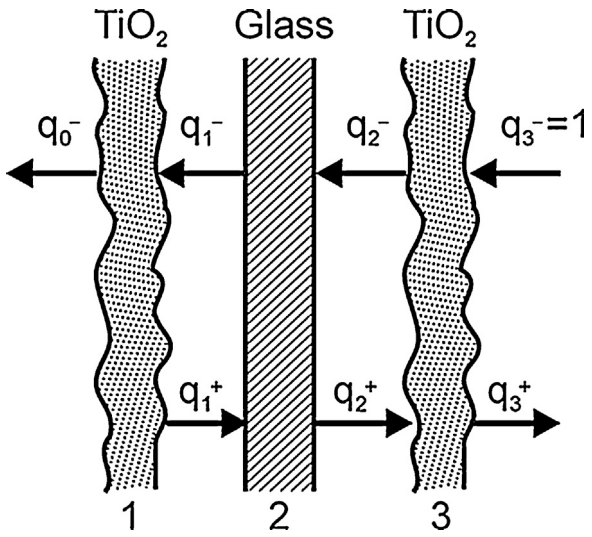

Fig. 5 – Schematic representation of the immobilized TiO_2 on glass during the optical properties measurements.

Then, the absorption radiation fraction can be calculated as follows (Siegel and Howell, 2002):

$$A_{TiO_2} = 1 - R_{TiO_2} - T_{TiO_2} \tag{7}$$

The calculated absorption fraction for the different tested samples together with the spectral emission distribution of the employed lamps can be found in Figs. 6 and 7 for the coatings on the smooth and sandblasting glasses respectively.

As it can be observed in Fig. 6, the fraction of energy absorbed by the commercial photocatalytic solutions is significantly lower than the TiO_2 powders absorption. On the other hand, the TiO_2 doped with carbon and 4 layers presents better radiation absorption on both smooth (Fig. 6) and sandblasted (Fig. 7) glasses. However, comparing the results in Figs. 6 and 7 for TiO_2-C and TiO_2-N samples and 4 layers, the sandblasting samples prepared with a TiO_2 suspension at pH equal to 1 present a significantly lower radiation absorption capability than the samples prepared on smooth glass with a natural pH suspension. This last is due to the TiO_2 suspension prepared at pH 1 presents smaller particle agglomerates and a less amount of catalyst deposited on the sandblasted glass (see Table 1).

In average, the TiO_2-C absorbed 32% and 20% more radiation than the TiO_2-N for the smooth and sandblasted samples respectively.

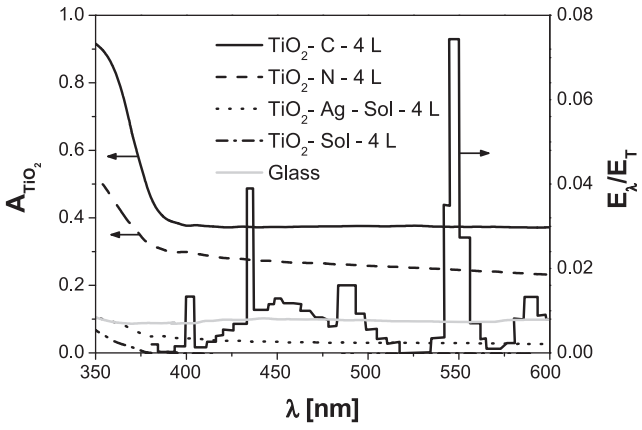

Fig. 6 – Spectral fraction of energy absorbed by the immobilized TiO_2 on smooth glass and the spectral emission distribution of the Philips lamps.

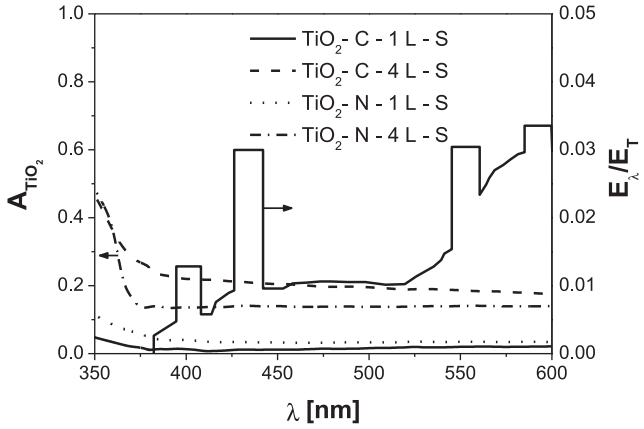

Fig. 7 – Spectral fraction of energy absorbed by the immobilized TiO_2 on sandblasted glass and the spectral emission distribution of the GE lamps.

3.2. *Nitrogen oxide degradation*

The photocatalytic oxidation of NO_x mixtures is reported in several publications (Devahasdin et al., 2003; Shelimov et al., 2008; Wang et al., 2007). All of them proposed the NO decomposition to NO_2, and then NO_2 to HNO_3 through the hydroxyl radical attack generated during the photocatalyst activation stage. For the reacting system applied here, fed with NO, NO_2 generation was observed as a reaction intermediate. As a result, the NO_x ($NO + NO_2$) concentration is higher than the NO concentration at the reactor outlet.

The NO and NO_x conversions for all samples on smooth glasses are reported in Table 3 and calculated according to:

$$X_i[\%] = \frac{C_{in,i} - C_{out,i}}{C_{in,i}} \times 100 \quad (8)$$

where i indicates NO or NO_x ($NO + NO_2$), and C_{in} and C_{out} are the reactor inlet and outlet concentration, respectively.

The samples prepared with the two commercial photocatalytic solutions did not show a significant NO_x reduction (less than 2%). So, these samples were not considered for further analysis.

Fig. 8 shows the total NO_x and NO concentration during the test for the carbon and nitrogen doped TiO_2 immobilized on the smooth glasses. Clearly, the carbon doped TiO_2 has shown a better photocatalytic performance for the NO_x degradation than the nitrogen doped TiO_2 powder. Meanwhile the total NO_x conversion by the TiO_2-C was about 18%, the TiO_2-N presented only 6% of NO_x degradation (Table 3).

In Table 4, three parameters related with the photocatalytic performance of the samples are reported. The first one is the average reaction rate in the photoreactor, calculated as:

$$\langle r_i \rangle_R = \frac{Q(C_{in,i} - C_{out,i})}{A_{int}} \quad (9)$$

Table 3 – Contaminant and total conversions.

Sample name	X_{NO}	X_{NOx}	X_{Acet}	$X_{Min,Acet}$
TiO_2-C-4 L	65.31	18.47	97.88	89.13
TiO_2-C-4 L-S	–	–	77.67	70.53
TiO_2-N-4 L	10.75	6.13	88.09	83.00
TiO_2-N-4 L-S	–	–	51.06	44.67
TiO_2-Ag-Sol-4 L	1.88	1.12	0.00	0.00
TiO_2-Sol-4 L	1.76	0.58	0.00	0.00

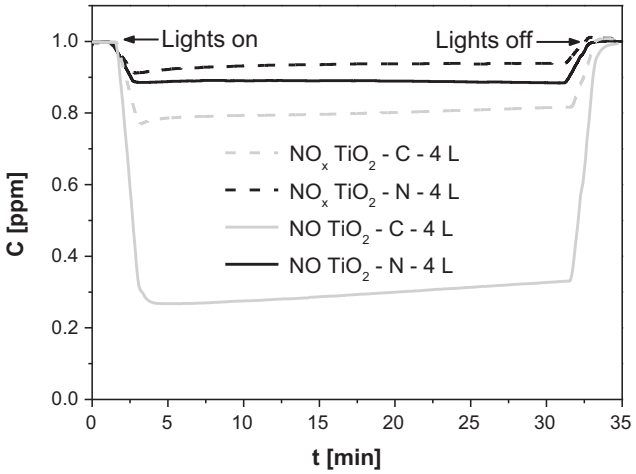

Fig. 8 – NO_x and NO outlet concentration evolution for the carbon and nitrogen doped TiO_2.

where Q is the gas flow rate in the photoreactor and A_{int} is the catalytic interfacial area. The calculated average reaction rate can be assumed free of external and internal mass transport limitations according to Appendix B.

The second parameter, the apparent photonic efficiency, is calculated as (Imoberdorf et al., 2007; Passalía et al., 2013; Muñoz Batista et al., 2014):

$$\eta_{p,i} = \frac{\langle r_i \rangle_R}{\sum_\lambda q_{w,\lambda}} \quad (10)$$

where $\sum_\lambda q_{w,\lambda}$ is the total incident radiation flux on the catalytic wall expressed in Einstein $m^{-2}\,s^{-1}$.

Finally, in order to incorporate the effect of the effectively absorbed radiation by the catalyst, the true quantum efficiency is calculated according to Eq. (11) (Imoberdorf et al., 2007; Passalía et al., 2013; Muñoz Batista et al., 2014) and summarized in Table 4.

$$\eta_{q,i} = \frac{\langle r_i \rangle_R}{\sum_\lambda A_{TiO_2,\lambda} q_{w,\lambda}} = \frac{\langle r_i \rangle_R}{\sum_\lambda A_{TiO_2,\lambda} (E_\lambda / E_T) q_w} \quad (11)$$

The values of the parameters reported in Table 4 follow the same trend than the NO and NO_x conversion reported in Table 3 for both samples. However, the difference between the quantum efficiencies of TiO_2-N and TiO_2-C samples is clearly less important since the TiO_2-N catalyst absorbs less radiation than the TiO_2-C. Meanwhile the NO_x conversion, reaction rate and photonic efficiency for the TiO_2-N sample are about 70% lower than the TiO_2-C ones, the quantum efficiency is only 50% lower.

3.3. *Acetaldehyde degradation*

The global reaction pathway of the acetaldehyde photocatalytic degradation can be assumed as follows (Sauer and Ollis, 1996):

$$\text{Acetaldehyde} \rightarrow \text{Formaldehyde} \rightarrow \text{FormicAcid} \rightarrow CO_2 \quad (12)$$

However, in the studied system only trace amounts of formaldehyde were detected and no formic acid was present (within the detection limit of 0.2 ppm for the developed analytical method).

Table 4 – Average reaction rate, apparent photonic and true quantum efficiencies for nitrogen oxide degradation.

Sample name	$\langle r_{NO}\rangle_R \times 10^8$ mol m^{-2} s^{-1}	$\langle r_{NO_x}\rangle_R \times 10^8$ mol m^{-2} s^{-1}	$\eta_{p,NO} \times 10^3$	$\eta_{p,NO_x} \times 10^3$	$\eta_{q,NO} \times 10^3$	$\eta_{q,NO_x} \times 10^3$
TiO_2-C-4 L	7.28	2.06	1.64	0.46	5.36	1.52
TiO_2-N-4 L	1.20	0.68	0.27	0.15	1.28	0.73

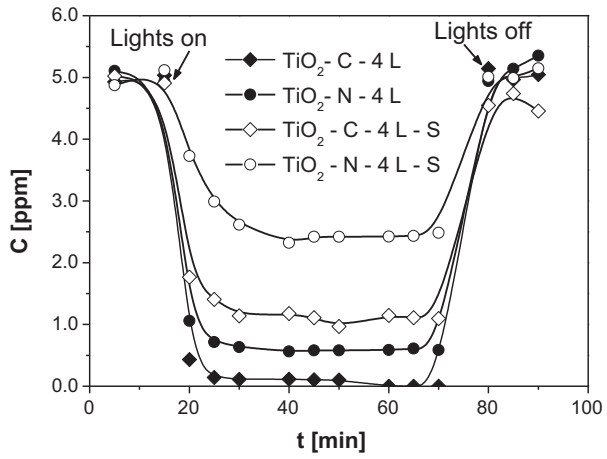

Fig. 9 – Acetaldehyde outlet concentration evolution for the carbon and nitrogen doped TiO_2 on smooth and sandblasted glass.

The degradation of acetaldehyde by the samples prepared on smooth or sandblasted glasses with the carbon and nitrogen doped TiO_2 can be compared in Fig. 9. For this contaminant, again the degradation by samples prepared with the commercial photocatalytic solutions is neglected compared with the carbon and nitrogen doped TiO_2.

In addition to the experimental results shown in Fig. 9, extra and longer tests were performed employing the sandblasted samples in order to evaluate the catalysts deactivation. After more than 10 h of reaction, the acetaldehyde degradation remained nearly constant.

Table 3 also reports the acetaldehyde conversion calculated according to Eq. (8) (with $i = Acet$) as well as the acetaldehyde total oxidation or mineralization ($X_{Min,Acet}$) that takes into account the formation of intermediates, calculated as:

$$X_{Min,Acet}[\%] = \frac{C_{in,Acet} - C_{out,Acet} - C_{out,Form}}{C_{in,Acet}} \times 100 \quad (13)$$

where $C_{out,Form}$ is the concentration of the formed formaldehyde at the reactor outlet.

Table 5 shows the acetaldehyde average reaction rates, and the apparent photonic and true quantum efficiencies.

Employing this contaminant, again the best de-pollution capability is observed for the TiO_2-C deposited on smooth glass, reaching almost 100% of conversion (Table 3). In this reaction system, two new samples prepared on sandblasted glasses and employing TiO_2-C and TiO_2-N powders suspension at pH 1 were tested. As discussed before, the amount of catalyst on this support was smaller, leading to a lower radiation absorption and therefore to a reduced acetaldehyde conversion.

In the same way that for the NO_x pollutant, the acetaldehyde conversion, reaction rate and photonic efficiency present the same trend if all samples are compared. However, the true quantum efficiency for the TiO_2-C-4L sample decreases significantly and its value becomes lower than for the rest of the samples. This last result is because an almost complete conversion was reached for the organic contaminant under the used operating conditions. In other words, as the acetaldehyde is consumed before is getting out of the reactor, for the TiO_2-C sample on smooth glass the effective catalyst reacting area is lower. Notice that for the calculation of the reaction rate the same area of 10×20 cm^2 was taken into account for all samples; consequently, the average reaction rate for TiO_2-C catalyst was underestimated leading to a lower quantum efficiency value.

Comparing the two reacting systems, the acetaldehyde conversion and reaction rate are significantly higher than the NO_x conversion using the smooth glass support. However, the acetaldehyde degradation for the nitrogen doped TiO_2 is exceeding the NO_x degradation by only a factor of 1.7 and 1.9 considering the apparent photonic and true quantum efficiencies respectively. On the contrary, for the case of the carbon doped TiO_2, the apparent photonic and true quantum efficiencies for the NO_x degradation is 1.6 and 1.5 respectively higher than for the acetaldehyde degradation due to, as mentioned before, the reaction rate for this sample was undervalued.

Anyhow, the true quantum and apparent photonic efficiencies for both reacting systems become more comparable than the respective reaction rates and conversions since the incident radiation flux in the acetaldehyde reacting system is higher than for the NO_x degradation.

A correlation between the obtained results for the photocatalytic performance and the fraction of energy absorbed by the immobilized TiO_2 powders can be observed. At the same time that the TiO_2-C absorbs about 32% more energy than TiO_2-N on smooth borosilicate glass, it could convert 66% more NO_x. On the other hand, using the sandblasted glasses, TiO_2-C also absorbs 20% more radiation than TiO_2-N and could degrade 37% more acetaldehyde. One of the reasons of the better performance of TiO_2-C can be attributed to its higher specific surface. However, it is worth to mention that other photocatalyst characteristics not studied here can influence its performance.

Table 5 – Average reaction rate, apparent photonic and true quantum efficiencies for acetaldehyde degradation.

Sample name	$\langle r_{Acet}\rangle_R \times 10^8$ mol m^{-2} s^{-1}	$\langle r_{Min,Acet}\rangle_R \times 10^8$ mol m^{-2} s^{-1}	$\eta_{p,Acet} \times 10^3$	$\eta_{p,Min,Acet} \times 10^3$	$\eta_{q,Acet} \times 10^3$	$\eta_{q,Min,Acet} \times 10^3$
TiO_2-C-4 L	9.10	8.28	0.31	0.28	1.11	1.01
TiO_2-C-4 L-S	7.22	6.56	0.25	0.22	1.74	1.58
TiO_2-N-4 L	8.19	7.71	0.28	0.26	1.49	1.40
TiO_2-N-4 L-S	4.75	4.15	0.16	0.14	1.56	1.36

4. Conclusions

The performance of different commercial modified TiO_2 photocatalysts was assessed under visible light for their application for air decontamination. Two representative air pollutants, nitrogen oxide and acetaldehyde, were successfully degraded for two of the four catalyst tested, the carbon and nitrogen doped TiO_2 powders.

The radiation absorption fraction of the immobilized catalysts was calculated from a radiation flux balance model and using the experimental values of diffuse reflectance and diffuse transmittance measurements.

The de-polluting performance of the selected catalysts for both inorganic and organic reacting systems was evaluated calculating the apparent photonic and the true quantum efficiencies. A correlation between the photocatalytic pollutants degradation and the immobilized TiO_2 optical properties was also found. These results are useful to appraise which TiO_2 will be more efficient for a full scale air decontamination process under indoor conditions. Particularly, under the tested operating conditions employed in the present work, the carbon modified photocatalyst promises a better performance for a real application.

Acknowledgements

Thanks are given to Universidad Nacional del Litoral, CONICET and Agencia Nacional de Promoción Científica y Tecnológica for the financial support (Argentina). Antonio Negro, Juan Andini, Claudio Passalía and Eduardo Vidal are acknowledged for their help during the experimental work at INTEC. The authors wish to express their thanks to the following sponsors of the research group at Eindhoven University of Technology (The Netherlands): Rijkswaterstaat Centre for Infrastructure, Graniet-Import Benelux, Kijlstra Betonmortel, Struyk Verwo, Attero, Enci, Provincie Overijssel, Rijkswaterstaat Directie Zeeland, A&G Maasvlakte, BTE, Alvon Bouwsystemen, V.d. Bosch Beton, Selor, Twee "R" Recycling, GMB, Schenk Concrete Consultancy, Intron, Geochem Research, Icopal, BN International, APP All Remove, Consensor, Eltomation, Knauf Gips, Hess ACC Systems and Kronos (in chronological order of joining). Qingliang Yu, Przemek Spiesz, Stepan Lorencik and Peter Cappon are acknowledged for the assistance during the experimental work at Eindhoven University of Technology.

Appendix A. Appendix A

According to Eq. (1), it can be written:

$$q_0^- = T_1 q_1^- + R_1 q_0^+ = T_{TiO_2} q_1^- \tag{A.1}$$

$$q_1^- = T_2 q_2^- + R_2 q_1^+ = T_g q_2^- + R_g q_1^+ \tag{A.2}$$

Then, considering a system conformed by only one layer (layer 1), q_1^+ can be expressed according to:

$$q_1^+ = R_1 q_1^- = R_{TiO_2} q_1^- \tag{A.3}$$

Replacing Eq. (A.3) into Eq. (A.2) and vice versa, the following expressions can be obtained respectively:

$$q_1^- = \frac{T_g q_2^-}{1 - R_g R_{TiO_2}} \tag{A.4}$$

$$q_1^+ = \frac{R_{TiO_2} T_g q_2^-}{1 - R_g R_{TiO_2}} \tag{A.5}$$

Also expressing q_2^- according to Eq. (1):

$$q_2^- = T_3 q_3^- + R_3 q_2^+ = T_{TiO_2} + R_{TiO_2} q_2^+ \tag{A.6}$$

Now, considering a system conformed by two layers (layers 1 and 2) the out coming flux q_2^+ can be expressed according to:

$$q_2^+ = R_{1,2} q_2^- = R_{TiO_2,g} q_2^- \tag{A.7}$$

In the same way as before, the following expression for q_2^- and q_2^+ can be derived:

$$q_2^- = \frac{T_{TiO_2}}{1 - R_{TiO_2} R_{TiO_2,g}} \tag{A.8}$$

$$q_2^+ = \frac{R_{TiO_2,g} T_{TiO_2}}{1 - R_{TiO_2} R_{TiO_2,g}} \tag{A.9}$$

Replacing Eq. (A.8) into Eq. (A.4):

$$q_1^- = \frac{T_g T_{TiO_2}}{(1 - R_g R_{TiO_2})(1 - R_{TiO_2} R_{TiO_2,g})} \tag{A.10}$$

Replacing Eq. (A.10) into Eq. (A.1):

$$q_0^- = \frac{T_g T_{TiO_2}^2}{(1 - R_g R_{TiO_2})(1 - R_{TiO_2} R_{TiO_2,g})} \tag{A.11}$$

Now considering the global transmittance of the three layer system composed by TiO_2, glass and TiO_2:

$$q_0^- = T_{1,2,3} q_3^- = T_{TiO_2,g,TiO_2} \tag{A.12}$$

Then, substituting Eq. (A.11) into Eq. (A.12), one can write:

$$T_{TiO_2,g,TiO_2} = \frac{T_g T_{TiO_2}^2}{(1 - R_g R_{TiO_2})(1 - R_{TiO_2} R_{TiO_2,g})} \tag{A.13}$$

Performing a radiation flux balance in the third layer, according to Eq. (2) we obtain:

$$q_3^+ = R_3 q_3^- + T_3 q_2^+ = R_{TiO_2} + T_{TiO_2} q_2^+ \tag{A.14}$$

Replacing Eq. (A.9) into Eq. (A.14):

$$q_3^+ = R_{TiO_2} + \frac{R_{TiO_2,g} T_{TiO_2}^2}{1 - R_{TiO_2} R_{TiO_2,g}} \tag{A.15}$$

Now considering the reflectance of the whole system:

$$q_3^+ = R_{1,2,3} q_3^- = R_{TiO_2,g,TiO_2} \tag{A.16}$$

Substituting Eq. (A.15) into Eq. (A.16):

$$R_{TiO_2,g,TiO_2} = R_{TiO_2} + \frac{R_{TiO_2,g} T_{TiO_2}^2}{1 - R_{TiO_2} R_{TiO_2,g}} \tag{A.17}$$

Table B1 – Estimation of internal and external mass transfer modulus.

Sample name	Nitrogen oxides		Acetaldehyde	
	Internal mass transfer modulus	External mass transfer modulus	Internal mass transfer modulus	External mass transfer modulus
TiO_2-C-4 L	5.03×10^{-6}	3.95×10^{-2}	2.06×10^{-4}	4.89×10^{-2}
TiO_2-C-4 L-S	–	–	1.33×10^{-6}	3.24×10^{-2}
TiO_2-N-4 L	4.42×10^{-7}	1.23×10^{-2}	1.01×10^{-5}	4.02×10^{-2}
TiO_2-N-4 L-S	–	–	1.70×10^{-7}	1.75×10^{-2}

By symmetry, applying the same procedure for a two layers system (conformed by TiO_2 and glass) an equivalent expression for the global reflectance can be obtained:

$$R_{TiO_2,g} = R_g + \frac{R_{TiO_2} T_g^2}{1 - R_{TiO_2} R_g} \tag{A.18}$$

Then, replacing Eq. (A.18) into Eq. (A.13) and into Eq. (A.17), we have:

$$T_{TiO_2,g,TiO_2} = \frac{T_g T_{TiO_2}^2}{(1 - R_g R_{TiO_2})[1 - R_{TiO_2}(R_g + (R_{TiO_2} T_g^2/(1 - R_{TiO_2} R_g)))]} \tag{A.19}$$

$$R_{TiO_2,g,TiO_2} = R_{TiO_2} + \frac{T_{TiO_2}^2 \left(R_g + \left((R_{TiO_2} T_g^2)/(1 - R_{TiO_2} R_g)\right)\right)}{1 - R_{TiO_2} \left(R_g + (R_{TiO_2} T_g^2)/(1 - R_{TiO_2} R_g)\right)} \tag{A.20}$$

From Eqs. (A.19) and (A.20) the transmittance and reflectance of the TiO_2 film (T_{TiO_2} and R_{TiO_2}) can be solved as a function of the experimental values of transmittance and reflectance of the three layer system (T_{TiO_2,g,TiO_2} and R_{TiO_2,g,TiO_2}) and of the glass (T_g and R_g), obtaining Eqs. (5) and (6).

Appendix B. Appendix B

The influences of internal mass transfer can be assessed by using the modified Weisz–Prater Criterion, assuming a pseudo-first order reaction rate (Missen et al., 1999):

$$\frac{\langle r_i \rangle_R e^2}{D_e C_{is}} < 0.5 \tag{B.1}$$

where $\langle r_i \rangle_R$ is the average reaction rate calculated according to Eq. (9), "e" the photocatalytic film thickness, C_{is} the contaminant concentration on the catalytic surface, and D_e the effective diffusion coefficient.

The thickness of the deposited photocatalyst can be estimated as follows:

$$e = \frac{m_c}{A_{int} \rho_c (1 - \phi)} \tag{B.2}$$

where m_c is the deposited catalyst mass, ρ_c the solid catalyst density, and ϕ the porosity of the catalytic film.

The effective diffusion coefficient is defined as:

$$D_e = \frac{D^* \phi}{\tau} \tag{B.3}$$

where τ is the tortuosity and D^* is the global diffusion coefficient:

$$D^* = \frac{1}{((1/D_{i-air}) + (1/D_k))} \tag{B.4}$$

In Eq. (B.4), D_{i-air} is the molecular diffusion coefficient of the i-contaminant in air and D_k is the Knudsen diffusion coefficient:

$$D_k = 9700 r_p \left(\frac{T}{M_i}\right)^{1/2} \tag{B.5}$$

where r_p is the porous radio, T is the temperature and M_i is the molecular weight of the i-compound.

On the other hand, the external mass transport limitations can be neglected when the average reaction rate is much slower than the interfacial mass transfer (Walter et al., 2005):

$$\frac{\langle r_i \rangle_R}{k_S \langle C_i \rangle_R} < 0.1 \tag{B.6}$$

where k_s is the external mass transfer coefficient that can be calculated from:

$$Sh = \frac{k_S \ L_C}{D_{i-air}} \tag{B.7}$$

Shah and London (1974) proposed that for slits with one exchanging side, the Sherwood number (Sh) can be taken as equal to 5. The characteristic length (L_c) of this system can be assumed equal to the hydraulic diameter of the photoreactor.

Results of the external and internal modulus (Eqs. (B.1) and (B.6)) are shown in Table B1 for the two contaminants and the different samples employed in this work. According to the adopted criteria, both the external and internal mass transfer limitations can be safely neglected.

References

Asahi, R., Morikawa, T., Ohwaki, T., Aoki, K., Taga, Y., 2001. Visible-light photocatalysis in nitrogen-doped titanium oxides. Science 293, 269–271.

Ballari, M.M., Hunger, M., Hüsken, G., Brouwers, H.J.H., 2010. NO_x photocatalytic degradation employing concrete pavement containing titanium dioxide. Appl. Catal. B: Environ. 95, 245–254.

Banerjee, S., Pillai, S.C., Falaras, P., O'Shea, K.E., Byrne, J.A., Dionysiou, D.D., 2014. New insights into the mechanism of visible light photocatalysis. J. Phys. Chem. Lett. 5, 2543–2554.

Chatterjee, D., Dasgupta, S., 2005. Visible light induced photocatalytic degradation of organic pollutants. Photochem. Photobiol. C: Photochem. Rev. 6, 186–205.

Daghrir, R., Drogui, P., Robert, D., 2013. Modified TiO_2 for environmental photocatalytic applications: a review. Ind. Eng. Chem. Res. 52, 3581–3599.

Demeestere, K., Dewulf, J., Ohno, T., Herrera Salgado, P., Van Langenhove, H., 2005. Visible light mediated photocatalytic degradation of gaseous trichloroethylene and dimethyl sulfide on modified titanium dioxide. Appl. Catal. B: Environ. 61, 140–149.

Devahasdin, S., Fan, C., Li, J.K., Chen, D.H., 2003. TiO_2 photocatalytic oxidation of nitric oxide: transient behavior and reaction kinetics. J. Photochem. Photobiol. A: Chem. 156, 161–170.

Edwards, D.K., 1977. Solar absorption by each element in an absorber-coverglass array. Solar Energy 19, 401–402.
Fuerte, A., Hernández-Alonso, M.D., Maira, A.J., Martínez-Arias, A., Fernandez-Garcia, M., Conesa, J.C., Soria, J., 2001. Visible light-activated nanosized doped-TiO_2 photocatalysts. Chem. Commun. 24, 2718–2719.
He, A., Xie, L., Tu, J., Song, S., Liu, W., Liu, Z., Fan, J., Liu, Q., Chen, J., 2010. Visible light-induced degradation of phenol over iodine-doped titanium dioxide modified with platinum: role of platinum and the reaction mechanism. J. Phys. Chem. C 114, 526–532.
Hoffmann, M.R., Martin, S.T., Choi, W., Bahnemann, D.W., 1995. Environmental applications of semiconductor photocatalysis. Chem. Rev. 95, 69–96.
Ihara, T., Miyoshi, M., Ando, M., Sugihara, S., Iriyama, Y., 2001. Preparation of a visible-light-active TiO_2 photocatalyst by RF plasma treatment. J. Mater. Sci. 36, 4201–4207.
Ihara, T., Miyoshi, M., Iriyama, Y., Matsumoto, O., Sugihara, S., 2003. Visible-light-active titanium oxide photocatalyst realized by an oxygen-deficient structure and by nitrogen doping. Appl. Catal. B: Environ. 42, 403–409.
Iketani, K., Sun, R.-D., Toki, M., Hirota, K., Yamaguchi, O., 2004. Sol–Gel-derived $V_xTi_{1-x}O_2$ films and their photocatalytic activities under visible light irradiation. Mater. Sci. Eng. B 108, 187–193.
Imoberdorf, G.E., Cassano, A.E., Irazoqui, H.A., Alfano, O.M., 2007. Simulation of a multi-annular photocatalytic reactor for degradation of perchloroethylene in air: parametric analysis of radiative energy efficiencies. Chem. Eng. Sci. 64, 1138–1154.
I.S.O. 22197-1, 2007. Fine Ceramics (Advanced Ceramics, Advanced Technical Ceramics) ÷ Test Method for Air Purification Performance of Semiconducting Photocatalytic Materials ÷ Part 1: Removal of Nitric Oxide. International Standards Organization (ISO), Geneva, Switzerland.
I.S.O. 22197-2, 2011. Fine Ceramics (Advanced Ceramics, Advanced Technical Ceramics) ÷ Test Method for Air Purification Performance of Semiconducting Photocatalytic Materials ÷ Part 2: Removal of Acetaldehyde. International Standards Organization (ISO), Geneva, Switzerland.
Jo, W.K., Shin, M.H., 2010. Visible-light-activated photocatalysis of malodorous dimethyl disulphide using nitrogen-enhanced TiO_2. Environ. Technol. 31 (5), 575–584.
Jo, W.K., Yang, C.H., 2010. Visible-light-induced photocatalysis of low-level methyl-tertiary butyl ether (MTBE) and trichloroethylene (TCE) using element-doped titanium dioxide. Build. Environ. 45, 819–824.
Kisch, H., Macyk, W., 2002. Visible-light photocatalysis by modified Titania. ChemPhysChem 3, 399–400.
Kubacka, A., Colón, G., Fernández-García, M., 2009. Cationic (V, Mo, Nb, W) doping of TiO_2–Anatase: a real alternative for visible light-driven photocatalysts. Catal. Today 143, 286–292.
Kuo, C.S., Tseng, Y.H., Huang, C., Li, Y., 2007. Carbon-containing nano-titania prepared by chemical vapor deposition and its visible-light-responsive photocatalytic activity. J. Mol. Catal. A: Chem. 270, 93–100.
Lin, Y.-M., Tseng, Y.-H., Huang, J.-H., Chao, C.C., Chen, C.-C., Wang, I., 2006. Photocatalytic activity for degradation of nitrogen oxides over visible light responsive titania-based photocatalyst. Environ. Sci. Technol. 40, 1616–1621.
Missen, R.W., Mims, C.A., Saville, B.A., 1999. Introduction to Chemical Reaction Engineering and Kinetics. John Wiley and Sons, New York.
Missia, D.A., Demetriou, E., Michael, N., Tolis, E.I., Bartzis, J.G., 2010. Indoor exposure from building materials: a field study. Atmos. Environ. 44 (35), 4388–4395.
Muñoz Batista, M.J., Ballari, M.M., Kubacka, A., Cassano, A.E., Alfano, O.M., Fernandez García, M., 2014. Acetaldehyde degradation under UV and visible irradiation using CeO_2–TiO_2 composite systems: evaluation of the photocatalytic efficiencies. Chem. Eng. J. 255, 297–306.
Nakamura, I., Negishi, N., Kutsuna, S., Ihara, T., Sugihara, S., Takeuchi, K., 2000. Role of oxygen vacancy in the plasma-treated TiO_2 photocatalyst with visible light activity for NO removal. J. Mol. Catal. A: Chem. 161, 205–212.
Nishijima, K., Ohtani, B., Yan, X., Kamai, T., Chiyoya, T., Tsubota, T., Murakami, N., Ohno, T., 2007. Incident light dependence for photocatalytic degradation of acetaldehyde and acetic acid on S-doped and N-doped TiO_2 photocatalysts. Chem. Phys. 339, 64–72.
Passalía, C., Alfano, O.M., Brandi, R.J., 2013. Optimal design of a corrugated-wall photocatalytic reactor using efficiencies in series and computational fluid dynamics (CFD) modeling. Ind. Eng. Chem. Res. 52, 6916–6922.
Sakthivel, S., Kisch, H., 2003a. Daylight photocatalysis by carbon-modified titanium dioxide. Angew. Chem. Int. Ed. 42, 4908–4911.
Sakthivel, S., Kisch, H., 2003b. Photocatalytic and photoelectrochemical properties of nitrogen-doped titanium dioxide. ChemPhysChem 4, 487–490.
Sauer, M.L., Ollis, D.F., 1996. Photocatalyzed oxidation of ethanol and acetaldehyde in humidified air. J. Catal. 158, 570–582.
Shah, R.K., London, A.L., 1974. Thermal boundary-conditions and some solutions for laminar duct flow forced convection. J. Heat Transf. 96 (2), 159–165.
Shelimov, B.N., Tolkachev, N.N., Tkachenko, O.P., Baeva, G.N., Klementiev, K.V., Stakheev, A.Y., Kazansky, V.B., 2008. Enhancement effect of TiO_2 dispersion over alumina on the photocatalytic removal of NO_x admixtures from O_2 to N_2 Flow. J. Photochem. Photobiol. A: Chem. 195, 81–88.
Siegel, R., Howell, J., 2002. Thermal Radiation Heat Transfer. Taylor and Francis, New York.
Van Durme, J., Dewulf, J., Sysmans, W., Leys, C., Van Langenhove, H., 2007. Efficient toluene abatement in indoor air by a plasma catalytic hybrid system. Appl. Catal. B: Environ. 74, 161–169.
Walter, S., Malmberg, S., Schmidt, B., Liauw, M.A., 2005. Mass transfer limitations in microchannel reactors. Catal. Today 110 (1–2), 15–25.
Wang, H., Wu, Z., Zhao, W., Guan, B., 2007. Photocatalytic oxidation of nitrogen oxides using TiO_2 loading on woven glass fabric. Chemosphere 66, 185–190.
Yu, Q.L., Brouwers, H.J.H., 2009. Indoor air purification using heterogeneous photocatalytic oxidation. Part I: experimental study. Appl. Catal. B: Environ. 92, 454–461.
Zacarías, S.M., Satuf, M.L., Vaccari, M.C., Alfano, O.M., 2012. Efficiency evaluation of different TiO_2 coatings on the photocatalytic inactivation of airborne bacterial spores. Ind. Eng. Chem. Res. 51, 13599–13608.